

## HIGH SPEED CURVING PERFORMANCE OF RAIL VEHICLES

Brian Marquis  
Robert Greif

Volpe National Transportation Systems Center  
US Department of Transportation  
Cambridge, MA, USA

### ABSTRACT

On March 13, 2013, the Federal Railroad Administration (FRA) published a final rule titled “Vehicle/Track Interaction Safety Standards; High-Speed and High Cant Deficiency Operations” which amended the Track Safety Standards (49 CFR Part 213) and the Passenger Equipment Safety Standards (49 CFR Part 238) in order to promote VTI safety under a variety of conditions at speeds up to 220 mph [1]. Among its main accomplishments, the final rule facilitates the expansion of higher speed passenger rail by revising the standards governing permissible operating speed in curves, allowing for higher cant deficiencies in all FRA Track Classes. To ensure safety is not diminished, the FRA Track Safety Standards require railroads to maintain their tracks to stricter track geometry standards whenever they operate at these higher curving speeds and cant deficiencies. These revisions were based on studies that examined the dynamic curving performance of various representative rail vehicles.

This research investigates the steady-state curving performance of truck designs while traversing curves at various curving speeds and cant deficiencies. During steady-state curve negotiation, the axles of trucks generally offset laterally from the track centerline and develop angles of attack increasing the wheel-rail contact forces. Large lateral forces can develop, particularly in flange contact, resulting in increased wheel and rail wear, track panel shift, and the risk of derailment. Depending on the truck design, such forces become larger at higher cant deficiency. An understanding of the steady-state response of a rail vehicle in a curve is essential as it represents a significant part of the total dynamic response.

The curving performance of an idealized rigid truck is analyzed using nonlinear analytical methods for a wide range of operating speeds and unbalance conditions. Emphasis is placed on higher speed curving and the results are used to interpret trends observed during recent field testing with Amtrak’s Acela High-Speed Trainset on the Northeast Corridor.

### INTRODUCTION

In this paper an examination is made of the steady-state curving of a rigid truck. In particular the effects of unbalanced applied forces, due to truck speed around curves, on the truck orientation and wheel forces are studied. For this analysis the rigid truck is modeled with wheels of constant conicity and vertical flanges. Several phases of truck configuration are investigated, low speed constrained curving, free curving, and high speed constrained curving. These are depicted in Figure 1. In Phase 1 – low speed constrained curving- the lead outer wheel and the trailing inner wheel of the truck are in flange contact. As the vehicle speed increases a point is reached for which the trailing inner wheel leaves flange contact, and equilibrium for steady-state curving is maintained with only the lead outer wheel in flange contact. This is denoted by Phase 2 in the figure. Finally as speed increases the trailing axle moves towards the outer rail, and at a critical speed value denoted as  $V_{transition}$ , both the trailing outer wheel and the leading outer wheel are in flange contact. This is denoted as Phase 3 high speed constrained curving in Figure 1. One of the primary results of the analysis is the magnitude and distribution of the wheel forces and their variation with vehicle speed and cant deficiency. While previous studies [2-4] focused on lower speeds (Phase 1, Phase 2), the present analysis provides insights into wheel forces at higher curving speeds (Phase 3).

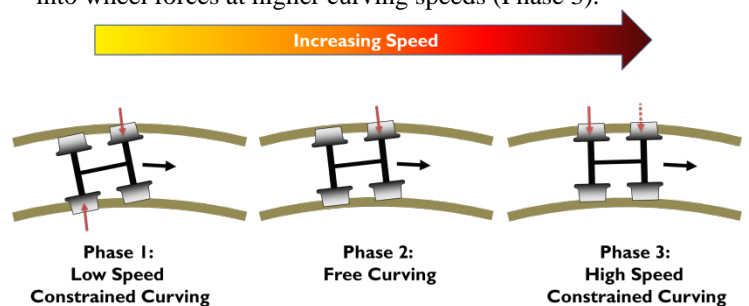


Figure 1: Rigid Truck Curving Phases

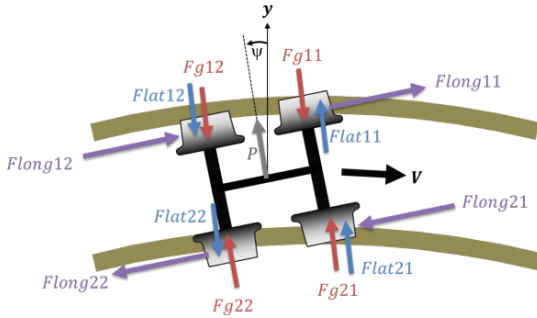
Of particular interest is the effect of speed on the lead axle flange force and whether this wheel remains in flange contact or pulls off from the outer rail (dashed red arrow Phase 3). Wherever possible, these results are compared with data from actual field testing on trains on the Northeast Corridor.

**NOMENCLATURE**

$V_{\text{transition}}$	speed at Phase 2 to Phase 3 transition
$f$	creep coefficient (units of force)
$E_a$	track superelevation
$F_{\text{long}}$	longitudinal creep force
$F_{\text{lat}}$	lateral creep force
$F_g$	flange force
$i, j$	$i = 1, 2$ outer, inner wheel; $j = 1, 2$ lead, trailing axle
$2L$	wheel spacing (approx. rail gauge)
$2hL$	wheelbase of truck (distance between axles)
$P$	net unbalance lateral load
$q$	flange clearance
$R$	radius of track curve
$r_0$	mean radius of wheel (undisplaced wheel)
$r$	radius of displaced wheel
$V$	velocity of truck
$y$	truck lateral displacement
$\alpha$	effective conicity of wheel
$\psi$	yaw angle of truck
$\mu$	coefficient of friction

**RIGID TRUCK ANALYSIS (FORCES, EQUILIBRIUM)**

A model of the rigid truck in curving with flange contact is shown in Figure 2 for Phase 2 curving with flanging on the lead outer wheel. The wheel creep forces are assumed proportional to the creep velocity (difference between actual and pure rolling velocity). These forces are in the lateral direction and tangential (or longitudinal) direction. Additionally, the figure shows the flange forces and the flange friction forces at the flange-rail contact point. The pertinent truck coordinates are the lateral displacement  $y$  and the yaw angle  $\psi$ .



$$\begin{aligned}
 Flat11 &= f \left( \frac{hL}{R+y} + \psi \right) & Flong11 &= f \left( \frac{\alpha}{r_0} (y + hL\psi) - \frac{L}{R+y} \right) \\
 Flat21 &= f \left( \frac{hL}{R+y} + \psi \right) & Flong21 &= f \left( \frac{\alpha}{r_0} (y + hL\psi) - \frac{L}{R+y} \right) \\
 Flat12 &= f \left( \frac{hL}{R+y} - \psi \right) & Flong12 &= f \left( \frac{\alpha}{r_0} (y - hL\psi) - \frac{L}{R+y} \right) \\
 Flat22 &= f \left( \frac{hL}{R+y} - \psi \right) & Flong22 &= f \left( \frac{\alpha}{r_0} (y - hL\psi) - \frac{L}{R+y} \right)
 \end{aligned}$$

**Figure 2: Steady-State Curving Forces on Rigid Truck**

An analysis is conducted based on equilibrium for the truck at a given speed  $V$  in a curve with constant radius  $R$ . The subscript notation  $i, j$  refers to the wheel, axle configuration with  $i=1, 2$  designating the outer or inner wheel, and  $j=1, 2$  designating the lead or trailing axle. The lateral force  $P$  acting on the truck is a combination of the centrifugal force associated with the truck speed and the gravity force. A calculation of  $P$  is based on Figure 3 for a carbody of weight  $W$  on a rigid suspension with the entire carbody-truck assembly oriented at an angle  $\theta$  to the ground due to superelevation  $E_a$ . Using the force components in the track plane, the net lateral force due to speed and weight is

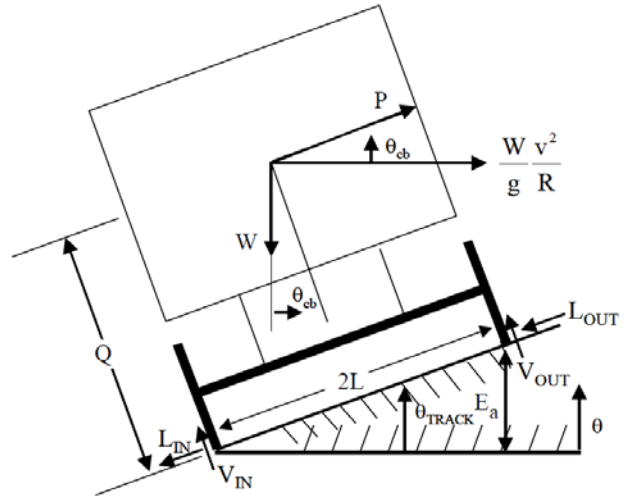


**Figure 3: Unbalance Lateral Force P**

$$P = \frac{mV^2}{R+y} \cos \theta - W \sin \theta \tag{1}$$

For typical track parameters

$$\sin \theta = \frac{E_a}{2L}, \quad \cos \theta \approx 1 \tag{2}$$

So that the lateral force can be written as

$$P = \frac{mV^2}{R+y} - W \frac{E_a}{2L} \tag{3}$$

For balance speed, the lateral force  $P$  is equal to zero. For speeds above balance speed, cant deficiency is the amount of additional superelevation (in inches) that would need to be added to the existing superelevation  $E_a$  in order to achieve balance [5].

Steady-state wheel/rail forces are calculated from the truck equilibrium equations which are established by summation of the wheel forces in the lateral direction and summation of moments for the forces shown in Figure 2. These equations are derived below for each of the three curving regions.

**Phase 1 Curving: Low Speed Constrained Curving**

Phase 1 curving consists of flange contact on the lead outer wheel and on the trailing inner wheel. The lateral and moment equilibrium equations are as follows:

$$4f\psi - Fg11 + Fg22 + P = 0 \tag{4}$$

$$-Fg11\left(1 + \frac{\mu}{h}\right)hL - Fg22\left(1 - \frac{\mu}{h}\right)hL - 4fL\left(\frac{\alpha}{r_o}\right)y + 4fL^2\left(\frac{1 + h^2}{(R + y)}\right) = 0$$

In this phase, the following geometric constraints are present:  $y = 0$  and  $\psi=q/hl$ , with  $q$  representing the flange clearance..

**Phase 2 Curving: Free Curving**

Phase 2 curving consists of flange contact on the lead outer wheel only. The lateral and moment equilibrium equations are as follows:

$$4f\psi - Fg11 + P = 0 \tag{5}$$

$$-Fg11\left(1 + \frac{\mu}{h}\right)hL - 4fL\left(\frac{\alpha}{r_o}\right)y + 4fL^2\left(\frac{1 + h^2}{(R + y)}\right) = 0$$

In this phase, the following geometric constraints are present:  $y+hL\psi=q$ , with  $q$  representing the flange clearance.

**Phase 3 Curving: High Speed Constrained Curving**

Phase 3 curving consists of flange contact on the lead outer wheel and on the trailing outer wheel. The lateral and moment equilibrium equations are as follows:

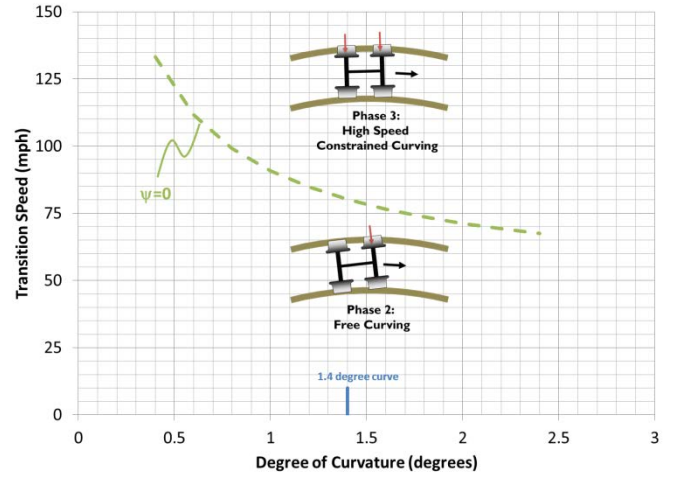
$$4f\psi - Fg11 - Fg12 + P = 0 \tag{6}$$

$$-Fg11\left(1 + \frac{\mu}{h}\right)hL + Fg12\left(1 - \frac{\mu}{h}\right)hL - 4fL\left(\frac{\alpha}{r_o}\right)y + 4fL^2\left(\frac{1 + h^2}{(R + y)}\right) = 0$$

In this phase, the following geometric constraints are present:  $\psi=0$  and  $y=q$ , with  $q$  representing the flange clearance. The calculations presented in this paper assume that these constraints on yaw and lateral displacement are constant for all Phase 3 curving speeds greater than  $V_{transition}$ . In reality these displacements have a small variation with speed and thus a small effect on the force results.

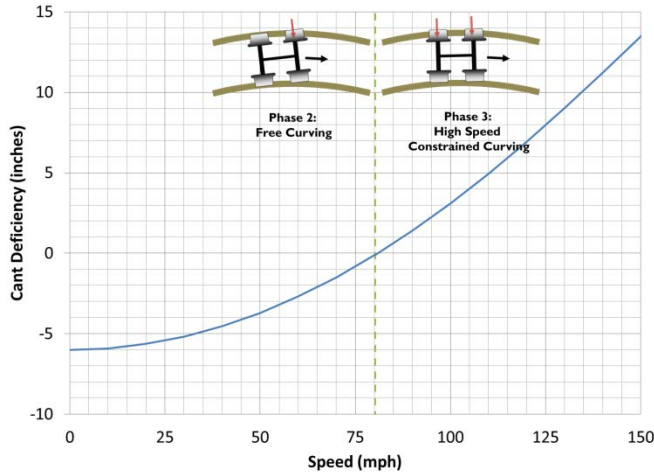
**RESULTS**

Figure 4 shows transition speed ( $V_{transition}$ ) for a rigid truck calculated in a range of curves with 5 inches of superelevation and varying degrees of curvature. A vehicle weight of 200,000 lbs and axle spacing of 112 inches are assumed. For this paper, results will be shown for a 1.4 degree curve (annotated in blue in Figure 4) in order to compare to results obtained during field testing with instrumented wheelsets on Amtrak’s Acela High-Speed Trainset. Results are presented as a function of speed (similar to repeat runs at different speeds in the testing, Figure 9). The transition speed for these conditions is 80 mph and is marked on each plot with a green vertical dashed line. Since the transition speed is defined here as the speed in which the truck switches between Phase 2 Curving and Phase 3 Curving, the equilibrium equations corresponding to Phase 2 were solved for speeds below the transition speed while the equilibrium equations corresponding to Phase 3 were solved for speeds above the transition speed.

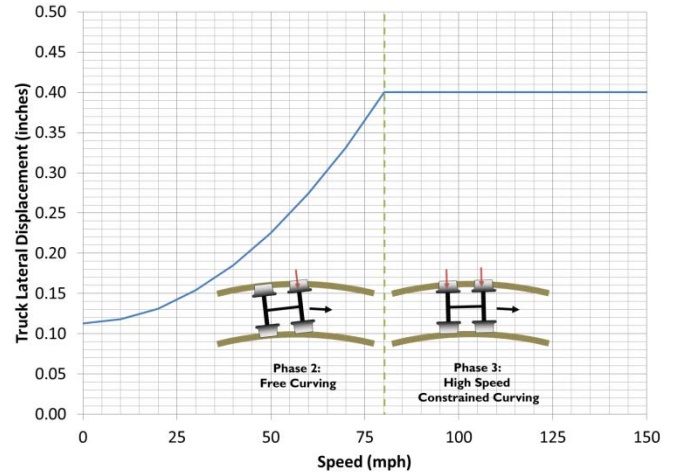


**Figure 4: Transition Speed**

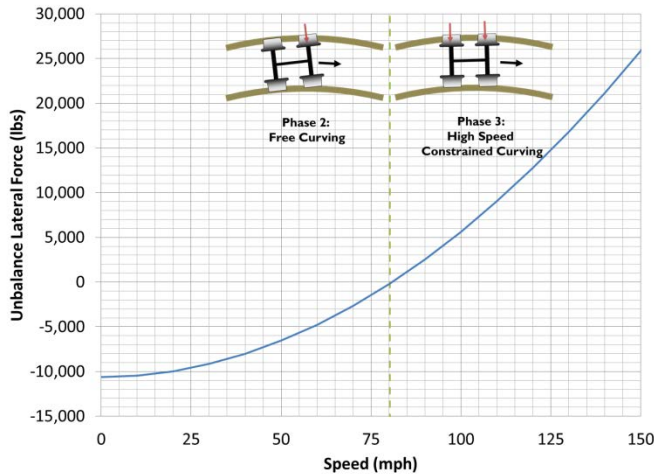
Figure 5 and Figure 6 respectively show the cant deficiency (inches) and unbalance force (lbs) while negotiating a curve with 1.4 degrees of curvature and 5 inches of superelevation at various speeds. The transition speed is generally close to the balance speed (i.e. the speed at which both the cant deficiency and unbalance force are zero), as shown in these figures for this particular case.



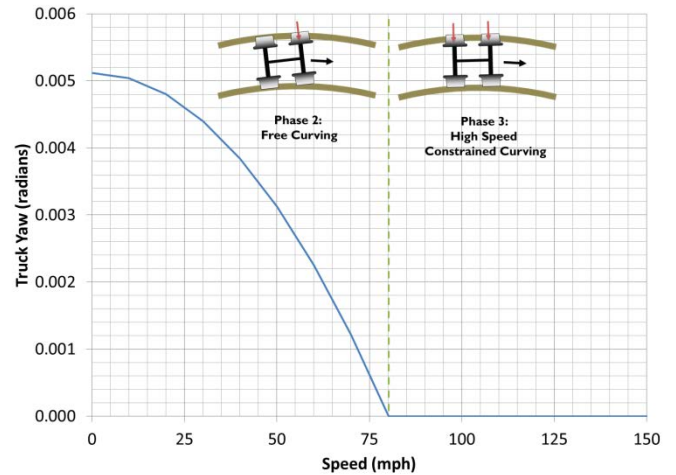
**Figure 5: Cant Deficiency**



**Figure 7: Truck Lateral Displacement**



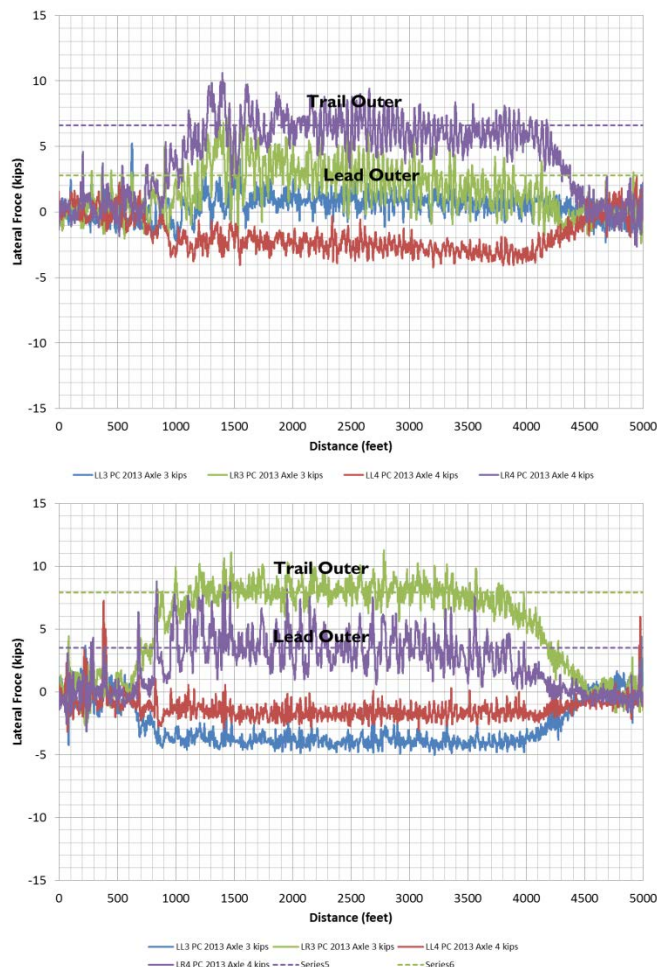
**Figure 6: Unbalance Force**



**Figure 8: Truck Yaw**

Figure 7 and Figure 8 respectively show the truck lateral displacement and yaw rotation needed to obtain steady-state equilibrium during curve negotiation in response to the unbalance force shown in Figure 6. The combination of these truck motions can displace the leading and trailing wheelsets laterally from their equilibrium rolling positions and/or orient them with a yaw rotation relative to the radial direction in a curve, producing longitudinal and lateral creep forces respectively. When displacements are large enough, flange contact will occur resulting in flange forces. The combination of creep forces and flange forces must balance and react the unbalance force. As mentioned previously, the calculations presented in this paper assume that these constraints on yaw and lateral displacement are constant for all Phase 3 curving speeds greater than  $V_{\text{transition}}$ . In reality these displacements have a small variation with speed and thus a small effect on the force results.

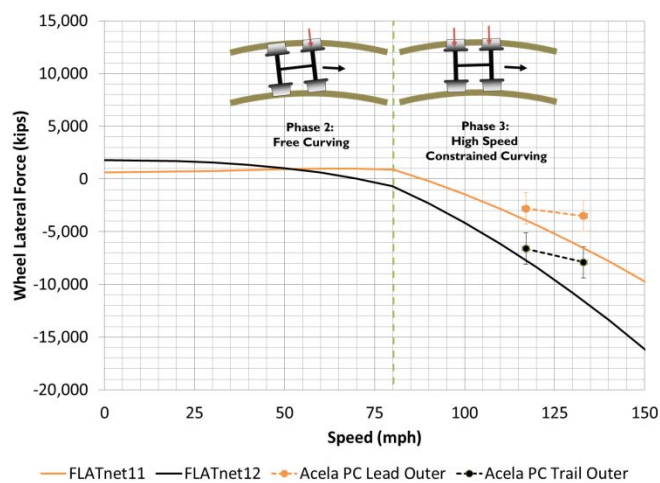
Figure 9 shows net lateral wheel forces (flange plus tread) measured during Acela Powercar (PC) testing in a curve with 1.4 degree curvature on Amtrak's Northeast Corridor. The forces are shown for each of the four wheels in a single truck at 2 higher curving speeds, 117 mph and 133 mph. During testing it was noted that the trailing axle outer lateral wheel force was larger than the leading axle outer at both speeds and that both wheels may be flanging. These field observations could not be explained by considering the mechanics of Phase 2 curving. This paper illustrates how these trends in the higher curving speed region can be explained considering the mechanics of Phase 3 curving.



**Figure 9: Acela PC IWS Test Data in 1.4 deg. curve:  
Run 1 = 117 mph (top), Run 2 = 133 mph (bottom)**

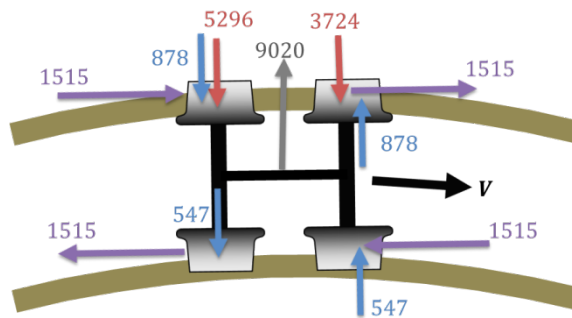
Figure 10 shows the predicted net lateral force (flange plus tread) on each of the outer wheels in a truck as well as the corresponding average measured forces from Figure 9 (dashed lines), with sign convention adjusted for comparison. The net lateral force represents the sum of creep force and flange force (if present) on each wheel. Although the analytical calculation predicts larger forces than the measured data due to uncertainties about the actual field conditions (friction, worn wheel/rail profile, speed, etc.) and to the assumptions of perfectly rigid truck, idealized wheel profile, and simplified creep force model, the results provide insights into the trends and overall higher speed curving behavior. Two important results are noted for speeds in Phase 3 Curving – namely, (1) the lead outer flange force, which is needed for equilibrium in Phase 2, is also needed for equilibrium in Phase 3 – i.e. the lead axle outer wheel remains in flange contact, and (2) as speed increases, the trail axle outer flange force is larger than the lead outer force. In Phase 3 curving, the flange forces (which are relatively low in Phase 2) are the dominant reaction forces needed to balance the unbalance lateral force  $P$  and thus suddenly increase rapidly in this phase (proportional to the

square of the velocity). These results have important implications on curving performance (for example rail and wheel wear) and safety (wheel climb and track panel shift).



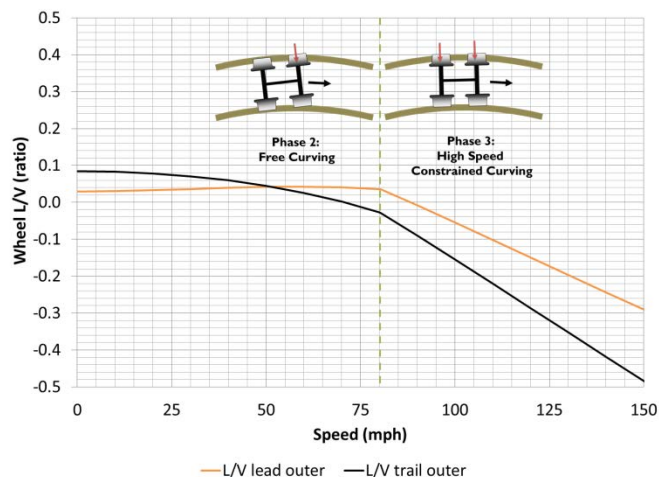
**Figure 10: Net Lateral Force on Wheel**

Figure 11 shows the free body diagram of the rigid truck showing the individual forces calculated at 110 mph. This Figure further illustrates that in order to satisfy both lateral and moment equilibrium above  $V_{transition}$  it is necessary for the lead outer wheel to remain in flange contact. Release of the lead outer flange force would result in a net counter clockwise moment and therefore moment equilibrium could not be maintained.



**Figure 11: Free Body Diagram of Rigid Truck at 110 mph.**

Figure 12 and Figure 13 respectively show the  $L/V$  on each of the outer wheels in the truck and the net axle lateral forces. These results show that the margin of safety from wheel climb derailment ( $L/V$ ) and track panel shift (net axle  $L/V$ ) decrease with increasing speed. At speeds much greater than the transition velocity, the increased forces on the trailing axle results in a higher risk of derailment.



**Figure 12: Wheel L/V**

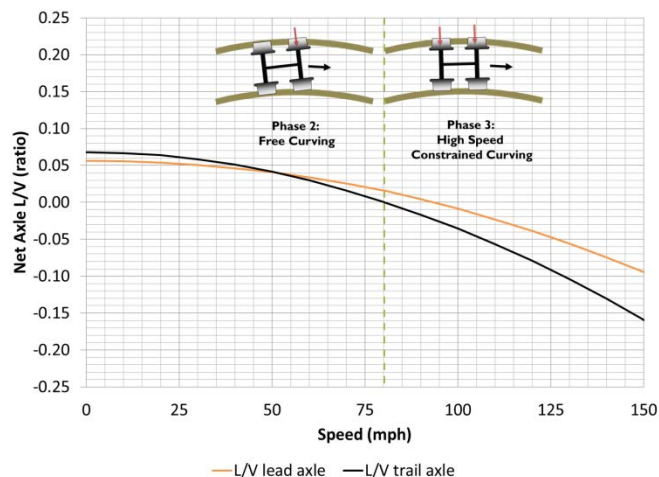


**Figure 13: Net Axle L/V**

## CONCLUDING REMARKS

This paper estimates the wheel-rail interaction forces and slip behavior of rigid trucks in curves with an emphasis on high-speed curving. Three phases of curving are described and analyzed. Two important results are noted for speeds in Phase 3 Curving – namely, (1) the lead outer flange force, which is needed for equilibrium in Phase 2, is also needed for equilibrium in Phase 3 – i.e. the lead axle outer wheel remains in flange contact, and (2) as speed increases, the trail axle outer flange force is larger than the lead outer force. These results have implications on curving performance (for example rail and wheel wear) and safety (wheel climb and track panel shift). The results also help to interpret recent trends observed with

wheel-rail interaction forces measured during instrumented wheelset testing with Amtrak’s Acela High-Speed Trainset on the Northeast Corridor. During this testing several passes were made at different speeds through the same curve. During these passes the wheel forces were larger on the trail outer wheels. An understanding of the steady-state response of a rail vehicle in a curve is essential as it represents a significant part of the total dynamic response, such as those shown in the field test.

To develop a better understanding of high speed curving behavior of various truck designs (Phase 3 curving), additional research is needed to understand if the conclusions reached in this study hold for other vehicle and track conditions. Future work will include additional field testing, model refinements and parametric studies. These efforts are intended to provide industry with insights into the relationships between key parameters and better curving performance at high speed operations.

## ACKNOWLEDGMENTS

The work described in this paper was sponsored by the Office of Research and Development, Federal Railroad Administration (FRA), U.S. Department of Transportation.

## REFERENCES

1. U.S. Department of Transportation, Federal Railroad Administration, 49 CFR Parts 213 and 238, Vehicle/Track Interaction Safety Standards; High-Speed and High Cant Deficiency Operations; Final Rule March 13, 2013.
2. Weinstock, H., and Greif, R., 1981, “Analysis of Wheel Rail Force and Flange Force During Steady State Curving of Rigid Trucks,” Proceedings of Joint ASME/IEEE Railroad Conference, April 28-30, 1981, Atlanta, Georgia, RT-81-5.
3. Newland, D.E., 1969, “Steering a Flexible Railway Truck on Curved Track”, Journal of Engineering for Industry, pp. 908 – 918.
4. Wickens, A., 2005, “Fundamentals of Rail Vehicle Dynamics”, CRC Press.
5. Marquis, B., Greif, R., and Curtis, E, 2005, “Effect of Cant Deficiency on Rail Vehicle Performance,” Proceedings of ASME International Design Engineering Technical Conferences & Computers and Information in Engineering Conference September 24-28, 2005, Long Beach, California, USA, DETC2005-85101.